Journal of Materials Chemistry A

ROYAL SOCIETY OF CHEMISTRY

PAPER

View Article Online
View Journal | View Issue

Check for updates

Cite this: J. Mater. Chem. A, 2024, 12, 29932

Polymorphism control of fast-sintered NASICON-type $LiZr_2(PO_4)_3$†

Lin Lin[a] and Kelsey B. Hatzell *[ab]

Received 29th June 2024
Accepted 24th September 2024

DOI: 10.1039/d4ta04507f

rsc.li/materials-a

Long processing times and high temperature sintering can lead to high energy intensities and costs for all solid state battery manufacturing. Fast-sintering methods that are compatible with air can potentially overcome these challenges. Dynamic pulses of electrified heat also provide a pathway for manipulating materials and material transformation pathways to provide more control over structural heterogeneity. Herein, we examine how ultra-fast sintering approaches impact polymorphism in NASICON-type solid electrolytes (*e.g.* $LiZr_2(PO_4)_3$). The role of microstructure (*e.g.* porosity), the polymorphism in starting powders, and the presence of liquid sintering aids are all examined to understand how polymorphic phases can be tailored with fast-sintering approaches. Fast sintering techniques which decrease the loss of volatile lithium may enable high density solid electrolytes with tailored material phases.

Introduction

All solid state batteries (ASSBs) are potentially safe and energy dense alternatives to conventional battery systems.[1–4] Utilizing a non-flammable, rigid solid electrolyte instead of a liquid electrolyte may enable the use of lithium metal or even lithium-free or reservoir free batteries.[5,6] However, scaling up solid electrolytes to meet the terrawatt demand is currently challenging.[7–9] Conventional solid-state synthesis and ceramic processing routes require large footprint manufacturing processes, high pressures, and long high temperature sintering. All of these contribute to the anticipated high cost of solid state batteries.

Chemically stable oxide ceramic materials that are stable with both high voltage cathodes and low voltage anodes are ideal for next generation batteries.[10,11] However, these ceramics typically have very high melting points and require high-temperature processing. Oxide solid electrolytes require high temperature sintering (>1000 °C) for hours or even days to achieve uniform densification. This long sintering process is challenging for lithium containing ceramics because lithium is highly volatile and can evaporate resulting in a solid electrolyte with stoichiometrically lean lithium. Less lithium results in poor transport properties. To overcome this challenge, it is common to cover the ceramic materials in a mother powder to decrease the loss of lithium.[12] This leads to excess waste and is not scalable.[13] The development of fast sintering techniques opens a new avenue for manufacturing and processing solid electrolytes with high throughput. These methods include flash sintering,[12,14] spark plasma sintering (also known as electric field assisted sintering),[15] low-temperature sintering,[16] microwave sintering,[17] and ultrafast high-temperature sintering.[12] However, many of these methods suffer from low heating rates, inert working environments, and expensive control systems.

In this work, we developed a modified air-compatible ultra-fast high temperature sintering method capable of sintering lithium conducting NASICON electrolytes in minutes. Fast sintering is capable of controlling polymorphic phases in these families of solid electrolytes. Control over solid electrolyte polymorphs can enable a dynamic way to tailor transport properties (*e.g.* ionic conductivity) in these materials. Stabilizing and promoting the highly conducting α-rhombohedral phase at room temperature is investigated with varying fast sintering profiles. The polymorphic density of a sintered solid electrolyte is affected by the porosity, grain size, heating rate, and structural variability in the initial green powders.

Conventional ultra-high temperature sintering (UHS) utilizes carbon or graphite-based materials as heating elements.[12] Using carbon electrical contacts enables exceedingly high temperatures (*e.g.* ≥2000 °C) and high voltages. However, carbon can chemically react with the solid electrolyte and oxygen at elevated temperatures. This can lead to contamination of the solid electrolyte unless it is processed in an inert environment. This makes large-scale integration challenging. Replacing carbon heating elements with alloy materials (kanthal Fe–Cr–Al alloy) can enable fast sintering in air (Fig. 1a). Processing in air can enable scalable processing at low costs. In addition, sintering in air can suppress oxygen vacancies and deleterious side reactions with carbon. In practice, powders synthesized *via* conventional solid-state synthesis techniques[18,19] are typically

[a]Andlinger Center for Energy and the Environment, Princeton University, Princeton, NJ 08540, USA. E-mail: kelsey.hatzell@princeton.edu

[b]Department of Mechanical and Aerospace Engineering, Princeton University, Princeton, NJ 08540, USA

† Electronic supplementary information (ESI) available. See DOI: https://doi.org/10.1039/d4ta04507f

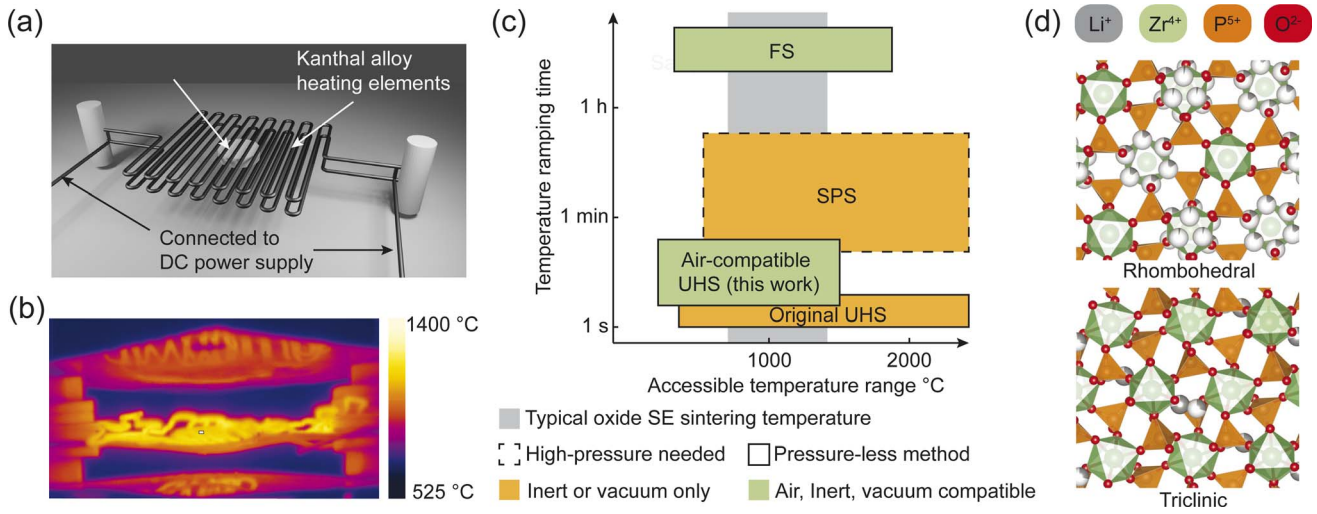

Fig. 1 (a) Schematic of the air-compatible ultra-high temperature sintering set-up. (b) Thermal image of the temperature profile across the sample during fast-sintering. (c) Comparison between different fast-sintering methods including flash sintering (FS), spark plasma sintering (SPS), original UHS and air-compatible UHS developed in this work. (d) Atomic arrangements of rhombohedral and triclinic polymorphic phases.

subjected to uniaxial pressure to form green body pellets. The pellets are then sandwiched between two kanthal coils, and a DC voltage is applied on both ends of the coils to enable rapid Joule heating bringing the pellet to about 1200 °C within 30 seconds as seen with a thermal camera (Fig. 1b and S1†). This allows sintering and rapid densification of solid electrolyte materials within minutes (>90% relative densities). The modified air-compatible UHS method enables high temperature ramping rates and is flexible to different environments (Fig. 1c). Fast ramp rates reduce the total energy cost when compared to spark-plasma sintering and conventional sintering (Fig. S2†).

Microstructure-driven polymorphism

NASICON-type $LiZr_2(PO_4)_3$ (LZP) is one type of solid electrolyte that demonstrates a relatively high bulk ionic conductivity. LZP demonstrates exceptional air and moisture stability similar to other NASICON-type Li-ion conductors such as $Li_{1+x}Al_xTi_{2-x}(PO_4)_3$ (LATP) and $Li_{1+x}Al_xGe_{2-x}(PO_4)_3$ (LAGP),[20] and demonstrates greater chemical compatibility with lithium metal than LATP and LAGP.[21] However, microstructural heterogeneity due to the grain size, grain boundaries, and polymorphism can drive a range of degradation mechanisms. Polymorphism or the presence of multiple phases of ion conducting materials can result in regions that are highly conducting and regions that have limited conductivity.[10] It has been reported that LZP can exhibit four different polymorphic phases: (1) α-rhombohedral, (2) α′-triclinic, (3) β-monoclinic, and (4) β′-tetragonal phases.[19,22–25] The β-monoclinic and β′-tetragonal phases are less common in solid electrolytes processed at high temperatures relevant for high density components. Instead, most reports studying LZP for battery applications report the α-rhombohedral or α′-triclinic phase (Fig. 1d).[26,27] The processing route,[22] precursors selection,[26] dopant,[28] particle size, and processing time and temperature can all influence the ratio of polymorphic phases in the final sintered solid electrolyte. Fast sintering approaches enable a rapid way to examine material transformation pathways and observe how polymorphism can be controlled.

The crystal structures of α-rhombohedral and α′-triclinic phases are very similar (Fig. 1d), making Rietveld refinement on X-ray diffraction (XRD) necessary for quantifying two phases (Fig. S3†). The α-rhombohedral phase has a higher symmetry and lithium ions are more equally distributed. The α′-triclinic phase has a slightly distorted Zr–P–O network which causes lithium ions to selectively occupy two distinct sites in the crystal. The ionic conductivity of the α-rhombohedral phase is 2 to 3 orders of magnitude greater than the α′-triclinic phase. Nevertheless, the α′-triclinic phase is thermodynamically more stable at room temperatures than the α-rhombohedral phase. Phase transformation between the α′-triclinic phase and α-rhombohedral phase occurs between 20 and 60 °C.[23,26,27] Thus, high-temperature processing steps will induce a phase transformation between the rhombohedral and triclinic phases and ultimately lead to a heterogeneous material system with a mixture of phases. Control and stabilization of the highly conducting α-rhombohedral phase at room temperature *via* dynamic processing conditions is of interest. One approach to obtaining higher concentrations of the rhombohedral phase is to sinter the sample for a longer time (Fig. S4†).[29] Sintering LZP using conventional high temperature furnaces (18 h/1200 °C) results in solid electrolytes with approximately 75% to 85% rhombohedral phases (Fig. S4†). Nevertheless, lithium is highly volatile at elevated temperatures, which possibly results in the loss of lithium during long sintering conditions. We also looked at the phase homogeneity within the sample, and observed that the rhombohedral phase distribution is homogeneous when the depth to the sample surface is greater than 0.2 mm (Fig. S5†).

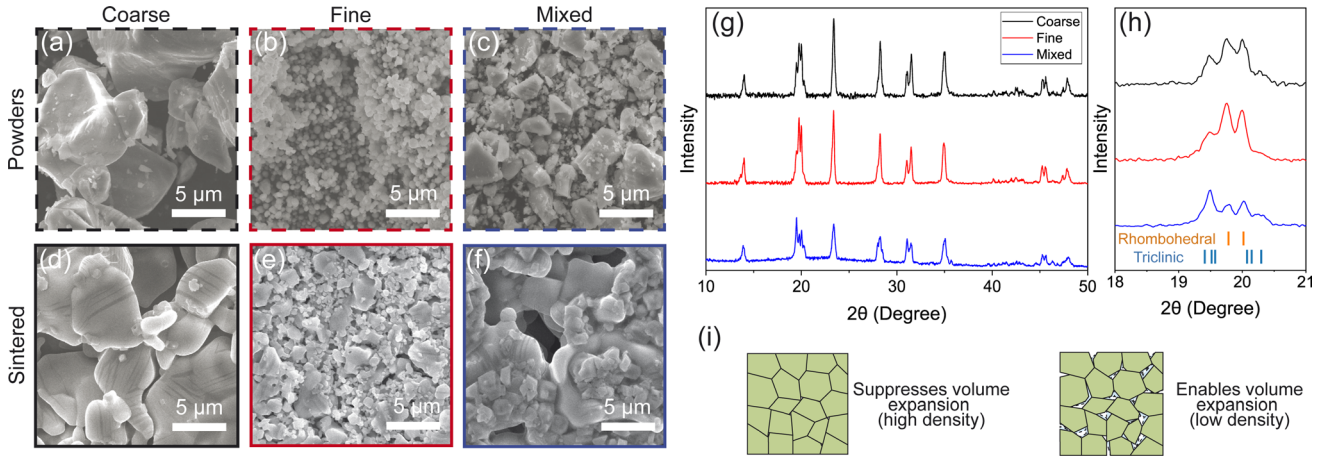

Fig. 2 Particle size effect on polymorphism. (a)–(c) SEM images for different particle sizes and uniformities used for pressing the pellet, with (a) coarse powders, (b) fine powders, and (c) mixed powders. (d)–(f) SEM images of sintered products from different powders, with (d) coarse powders, (e) fine powders, (f) and mixed powders. (g) XRD results and (h) zoomed-in results for the key peaks corresponding to triclinic and rhombohedral phases for pellets sintered from these particles, showing that the rhombohedral phase ratio increases as the powder particle size gets smaller and more uniform. (i) Stress-driven mechanism of rhombohedral phase stabilization, indicating lower porosity generally yields a higher rhombohedral phase ratio.

Table 1 Effect of particle size and the distribution of powders. The initial phase of the green bodies was kept to be triclinic (*i.e.*, no preheating step), and no sintering aid was used

Particle type and size	Rhombohedral phase ratio (%)	Diameter of sintered pellets (mm)	Relative density of sintered pellets (%)	RT ionic conductivity (S cm^{-1})
Coarse (10 μm)	65	5.95	75	5.0×10^{-6}
Fine (0.5 μm)	74	5.74	84	8.8×10^{-6}
Mixed (wide range of distribution)	42	6.05	70	4.1×10^{-8}

The rhombohedral phase has a higher density (3.15 g cm^{-2}) than the triclinic phase (3.11 g cm^{-2}).[19] Therefore, there will be a volume expansion within the pellet when the solid electrolyte transforms from the predominantly high-temperature stable phase (*e.g.* rhombohedral) to the predominantly low-temperature stable phase (*e.g.* triclinic). It has been hypothesized that the rhombohedral phase is likely stabilized at room-temperature in a stressed form instead of distorting to the thermodynamically stable triclinic phase.[18] Increasing the packing density (*e.g.* low porosity) of the green powders can lead to compressive stresses during densification and suppress the rhombohedral-to-triclinic volume expansion phase transformation pathway (Fig. 1d). To systematically explore the role porosity plays in this phase transformation we prepared three types of powders: (1) coarse (10 μm), (2) fine (0.5 μm), and (3) mixed (Fig. 2a–c). The mixed sample was composed of particles between 0.5 and 5 μm in diameter. Powder XRD confirmed that the predominant phase for all these powders is triclinic (Fig. S6†). Sintering pellets at 1200 °C for 2 min results in dense solid electrolytes (Fig. 2d–f). A greater concentration of rhombohedral phase is achieved with pellets processed from fine powders (*e.g.* dense electrolytes) when compared with the coarse powders (Fig. 2g and h, Table 1). The pellet sintered from the mixed powders produces solid electrolytes with the lowest rhombohedral phase ratio. The corresponding sample shrinkage (indicated by the diameter of sintered pellets) and relative density follow a similar trend (Table 1). The fine-powder pellets give the smallest diameter (highest shrinkage) and highest relative density, while the mixed-powder yields the highest diameter (lowest shrinkage) and lowest density, suggesting a stress-driven stabilization of the rhombohedral phase (Fig. 2i). Compared to the case of coarse powders, the green body pressed from fine powders likely achieves higher initial packing density as well as a higher sintering activity thanks to the much larger surface area.[30] For the case of mixed powders with a wide particle size distribution, as previously demonstrated, densification is likely prevented during sintering because of the increased contact area between particles which overcompensates the enhancement from particle rearrangement.[31]

Implications of powders in the green body

In addition to stress-driven impacts on phase transformations, the initial polymorphic phase composition in the green body

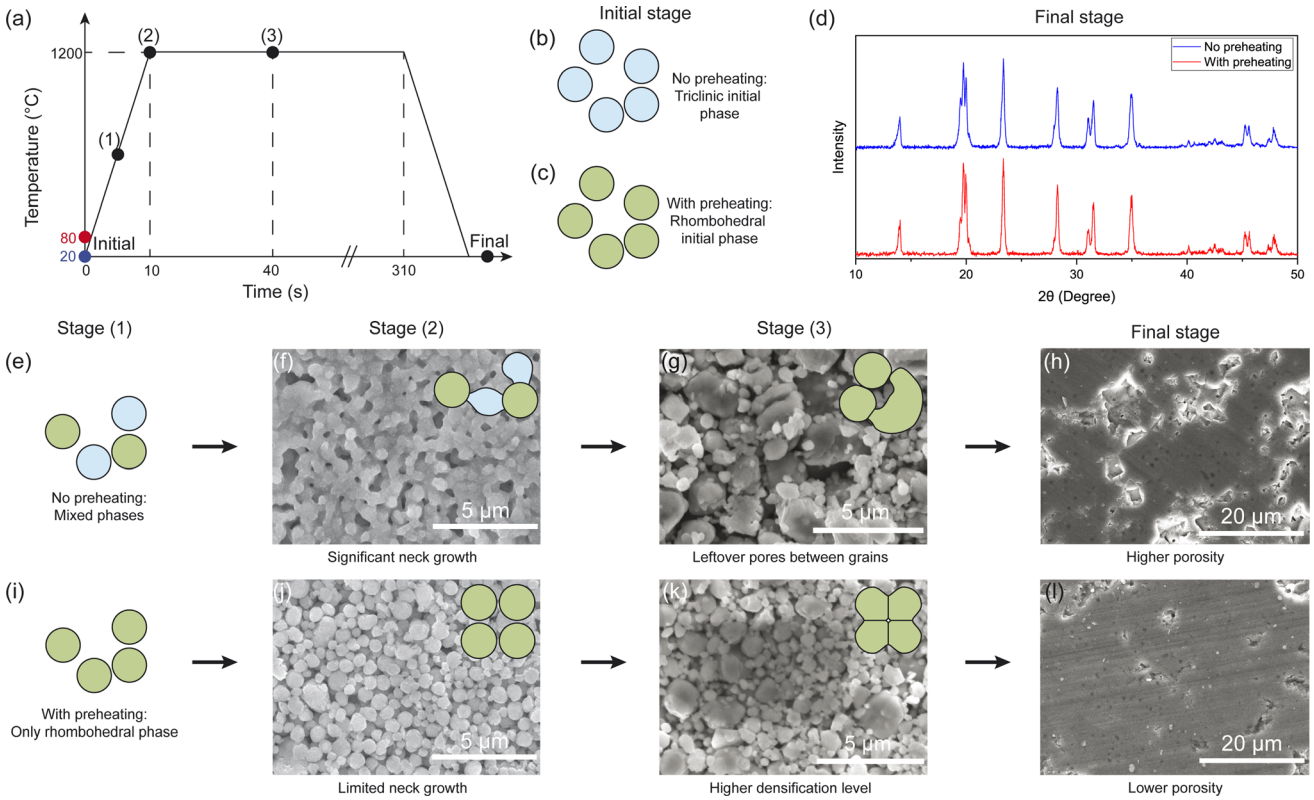

Fig. 3 The impact of the polymorphism in the starting green body on the densification and polymorphism of sintered products. (a) Schematic heating profile during UHS labeled with different heating stages. (b) Triclinic and (c) rhombohedral initial polymorphisms achieved without or with a preheating step. (d) XRD results for pellets sintered without and with preheating, indicating that the pellets sintered from a pure rhombohedral green body show a higher rhombohedral phase ratio in the final sintered product. At the rapid heating stage (1), the samples without preheating (e) demonstrate mixed polymorphic phases, whereas the sample with preheating (i) gives only a rhombohedral phase. At the initial sintering stage (2), the sample without preheating (f) shows more significant neck growth than its preheating counterpart (j), as indicated by SEM images. At the continued sintering stage (3), the sample without preheating (g) shows more uneven grain growth and more leftover pores between grains than the preheated one (k). At the final stage, the sample without preheating (h) yields higher porosity than the preheated sample (l), correlated with the final polymorphism difference.

Table 2 Effect of starting polymorphism of the green body. The particle size of the green bodies was kept to be fine, and no sintering aid was used

Starting polymorphism	Rhombohedral phase ratio (%)	Diameter of sintered pellets (mm)	Relative density of sintered pellets (%)	RT ionic conductivity (S cm^{-1})
Mixed	72	5.62	85	7.0×10^{-6}
Pure rhombohedral	81	5.43	93	1.5×10^{-5}

can also significantly affect densification mechanisms and the polymorphism of the sintered pellets. Green body LZP pellets pressed with powders synthesized *via* a conventional solid state reaction route demonstrate nearly a pure triclinic phase at room temperature (Fig. S7†). When the green body pellet is heated to over 60 °C, it transforms to an almost pure rhombohedral phase (Fig. S6†). This trend agrees with previous literature findings.[18,19,26] Therefore, the initial polymorphic phase ratio of the green body pellets can be controlled through simple preheating strategies (Fig. 3a and b). Preheating the green body (80 °C for 15 min) can result in a green body which is almost purely rhombohedral prior to sintering (Fig. 3c). Green bodies, subjected to the preheating step resulting in an initial concentration of rhombohedral phase, result in a greater shrinkage and higher density (95%) solid electrolyte (Table 2) after 5 min high-temperature sintering. A higher packing density likely assists in the stabilization of the rhombohedral phase. A rhombohedral phase ratio approaching 81% was achieved with green pellets sintered with a preheating stage. The absence of a preheating stage resulted in a lower rhombohedral phase ratio (72%) (Fig. 3d).

Ultra-fast high temperature sintering results in materials which experience ultrahigh heating rates (>10^3 °C min^{-1}). The LZP particles with a triclinic phase in the pressed green body experiencing such high heating rate will likely not have sufficient time to be converted to a rhombohedral phase. High

heating rates can lead to incomplete or non-uniform phase transformation throughout the thickness of the pellet, resulting in a mixture of rhombohedral and triclinic phases during the initial sintering step (Fig. 3a and e). Powders with non-uniform and uniform phase concentrations due to preheating experience different grain growth properties and microstructural transformations during densification, which are observed directly with scanning electron microscopy. Samples with mixed polymorphic phases show clear neck growth and coarsening between particles upon sintering (Fig. 3f). Upon further sintering the mixed phase, the green body shows more significant grain growth, grain size heterogeneity, and coarsening which all lead to an increase in the porosity of the ceramic (Fig. 3g and h). Powders with purely rhombohedral starting powders demonstrate more controlled grain growth processes and densification (Fig. 3i–l). The densification mechanism and phase transformation pathway for a pellet initially comprised of a high concentration of α-rhombohedral are very different from a pellet comprised of a mixture of α′-triclinic and α-rhombohedral phases.

The material transformation pathways experienced by the triclinic and rhombohedral phases during sintering differ drastically. From the SEM images on different sintering stages, it is plausible that the triclinic particles experience more significant grain coarsening and mass transportation. This may be attributed to several factors. The slightly lower density of the triclinic phase may result in residual porosity when a triclinic grain undergoes a phase transformation between the triclinic phase and the rhombohedral phase during high-temperature sintering. Moreover, there may be a surface energy difference between the two polymorphs, similar to what was previously observed in Y_2O_3 polymorphic systems.[32] A phase with a higher surface energy can initiate greater surface diffusion than the lower surface-energy phase (Fig. 3h) and result in neck growth.[33] Neck growth induces more significant grain growth and prevents densification in the mixed-phase sample by forming a vermicular-shaped grain network. Additionally, the pore redistribution during nucleation and growth of the rhombohedral phase from the triclinic phase might also create interconnected pore networks that are detrimental to densification.[34,35] All these factors can contribute to the lower porosity and lower rhombohedral phase ratio observed in the sample without the preheating stage. Given the unique high heating rate during ultrafast sintering, extra consideration on polymorphism of starting and final materials is needed to understand and control the sintering behaviors and materials performance.

Implications of liquid sintering aid on polymorphism

The transport and electrochemical properties of a solid electrolyte are greatly influenced by the electrolyte density, microstructure (grain size, grain boundary, *etc.*) and the stoichiometry of lithium. Lithium tends to occupy interstitial sites in LZP, and it has been suggested that higher lithium concentration in the interstitial sites aids in the stabilization of the rhombohedral phase.[18,22,36] High temperature sintering can lead to lithium evaporation which can reduce the concentration of the rhombohedral phase in the solid electrolyte and decrease transport properties. To explore the impact of lithium stoichiometry on the phase transformation pathway we combined the LZP powders with 10% molar ratio excess Li (Li_2CO_3). The excess mass ratio was around 0.78% (Li_2CO_3 to LZP). Solid electrolytes sintered with excess lithium achieved 85% rhombohedral phase after 5 minutes fast sintering, while solid electrolytes without the excess lithium only achieved 72% rhombohedral phase (Fig. 4a, Table 3). The solid electrolyte sintered with excess lithium also demonstrated greater shrinkage and a higher density (Table 3). This shows similarities in terms of relative density, rhombohedral phase ratio, and ionic conductivity (see

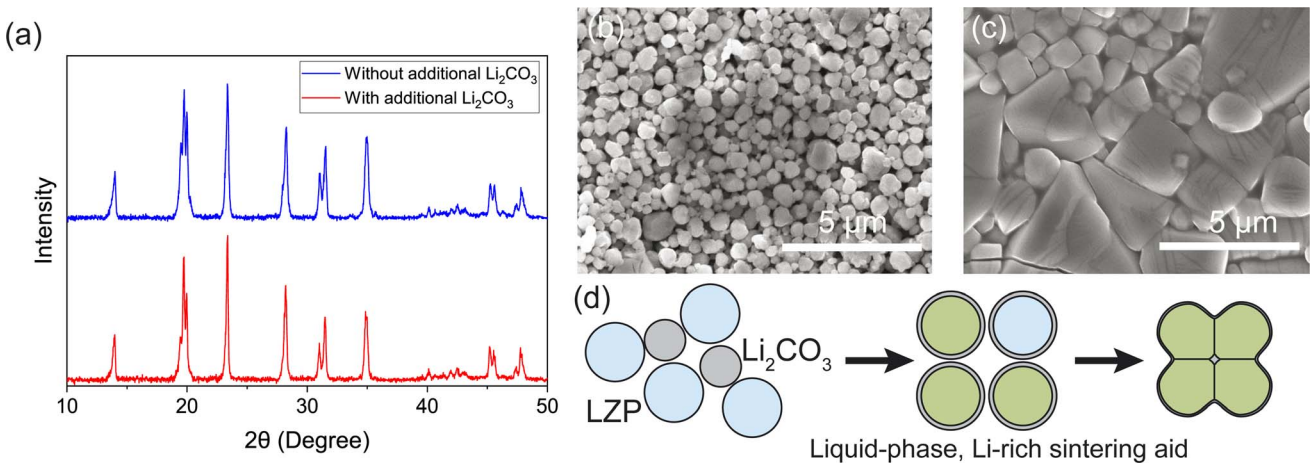

Fig. 4 Effect excess lithium on phase transformation in LZP solid electrolyte. (a) XRD results for pellets with and without Li_2CO_3 fast sintered at 1200 °C for 5 minutes. (b) SEM image of the initial sintering stage of a pellet with additional Li_2CO_3 in the green body, indicating limited neck growth. (c) SEM image of a pellet with additional Li_2CO_3 sintered at 1200 °C for 30 seconds, suggesting significant densification likely due to liquid phase sintering. (d) Schematic illustration of the role of added Li_2CO_3 in modifying surface energy to suppress neck growth and enabling liquid phase sintering.

Table 3 Effect of Li_2CO_3 as a sintering aid. The particle size in the green bodies was kept to be fine, and no preheating step was added

Li_2CO_3 addition status	Rhombohedral phase ratio (%)	Diameter of sintered pellets (mm)	Relative density of sintered pellets (%)	RT ionic conductivity (S cm^{-1})
Without Li_2CO_3	72	5.62	85	7.0×10^{-6}
With Li_2CO_3	85	5.45	95	1.3×10^{-5}

below) compared to the previously discussed samples with additional preheating. On the other hand, introduction of Li_2CO_3 rules out the need of having a pure rhombohedral green body. *Ex situ* imaging of the grain growth process during fast sintering sheds light onto the role the Li_2CO_3 plays in densification and grain growth during fast sintering. A solid electrolyte with excess lithium was heated to 1200 °C and then immediately cooled down to room temperature (within 10 seconds) and imaged using scanning electron microscopy (Fig. 4b) to understand the microstructural properties at the initial sintering stage. The solid electrolyte with additional Li_2CO_3 at this stage has very small grains with limited neck growth between adjacent grains, similar to the preheated sample described in the previous section. When the same solid electrolyte is held at 1200 °C for only 30 seconds we observe significant changes to the microstructure. Very large grains on the order of 1–5 μm are present after only 30 seconds of sintering (Fig. 4c). Li_2CO_3 can act as a liquid sintering aid and decompose to the Li_2O liquid and coat LZP particles. The liquid coating likely resists the microstructural evolution associated with the triclinic particles and limits surface diffusion and neck growth (Fig. 4d).

Control over polymorphic phases in LZP can be achieved *via* microstructural control (*e.g.* particle size), initial polymorphism control and the use of a sintering aid. All of these have been shown to be effective strategies for controlling the ratio of rhombohedral to triclinic polymorph in a LZP solid electrolyte. The ionic conductivity is directly correlated with the rhombohedral phase ratio in the solid electrolyte (Fig. S7†). This confirms previous reports which show that the rhombohedral phase is at least two orders of magnitude more conductive than the triclinic phase. The room temperature ionic conductivity of the 85% rhombohedral solid electrolyte is 1.3×10^{-5} S cm^{-1} which agrees with values reported by previous studies with room temperature rhombohedral phase stabilization.[22,26] The subtracted activation energy is about 0.40 eV for most of the ultrafast-sintered samples with a high rhombohedral phase ratio, whereas the pellets densified from coarse powders demonstrate a lower activation energy of 0.30 eV (Fig. 5 and

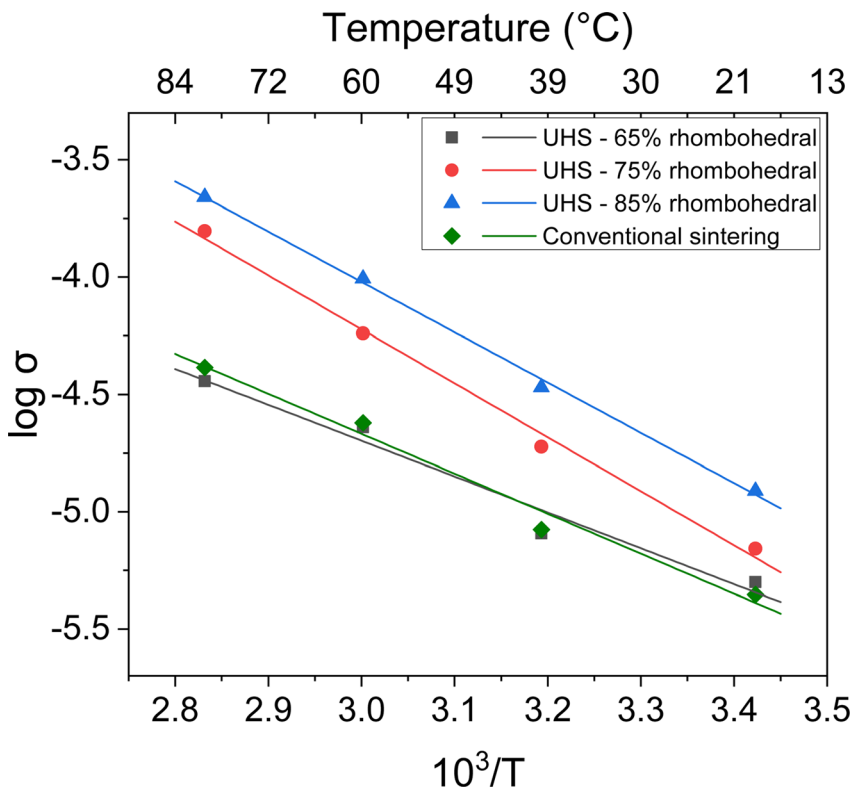

Fig. 5 Arrhenius plots corresponding to ionic conductivities of different samples, suggesting activation energies of 0.40 eV for the 75% and 85% rhombohedral ratio samples achieved by UHS, and 0.30 eV for the 65% sample prepared with coarse powders. The ionic conductivities of the conventionally sintered samples were also included, with an activation energy of 0.34 eV.

S8†). Meanwhile, the least ionic conductive sample is the one sintered from mixed powders, showing only 4.1×10^{-8} S cm^{-1} room temperature ionic conductivity, agreeing well with its very low rhombohedral phase ratio (44%) (Fig. S9†). The cycling stability testing results of Li|LZP|Li symmetric cells suggest that for LZP solid electrolytes with a rhombohedral phase ratio more than 75% (and associated high density), the cell voltage stability is relatively good with small voltage increase over time (Fig. S10†).

Conclusion

In this work, we systematically investigated how processing conditions and local phase transformation impact polymorphism in LZP. Using a modified air-compatible UHS approach we can systematically survey through a range of factors that impact densification and sintering. Control over the initial particle size, composition of green body polymorphism, and the presence of sintering aid impact the composition and transport properties of NASICON type solid electrolytes. The highly ionic conductive rhombohedral phase can be stabilized with (i) a smaller and more-uniform particle size, (ii) the addition of a preheating step immediately before sintering to transfer the green body to a pure rhombohedral phase, and (iii) the addition of Li_2CO_3 as a sintering aid. Such rhombohedral phase stabilization is likely a result of lower porosity and smaller grain sizes, which are achieved by the interplay of surface energy and the diffusion mechanism during ultra-fast high temperature sintering. This work provides guidance on controlling structural heterogeneity through advanced manufacturing of solid electrolyte materials.

Experimental

The LZP powders used for sintering were prepared *via* a conventional solid state reaction route. Basically, stoichiometric amounts of Li_2CO_3, $NH_4H_2PO_4$ and ZrO_2 were mixed together with a mortar and pestle. The mixture was placed in a Pt boat, and heated in a tube furnace at 500 °C for 1 h and 800 °C for 6 h to decompose precursors and evaporate CO_2, ammonia, and water vapor. The resulting white mixture was then heated at 1200 °C for 20 h to yield LZP powders.

Typically, the powders were ball-milled in a Fritsch Pulverisette 7 premium line planetary ball mill with ZrO_2 containers and balls at 350 rpm for 5 h, which yielded fine powders. The coarse powders were prepared by hand grinding the 1200 °C, 20 h fired products for 15 min with an agate mortar and pestle. The mixed powders were prepared by ball-milling the product from 1200 °C, 20 h heat treatment at 150 rpm for 2 h. The powders were then pressed into pellets *via* uniaxial pressing at 500 MPa to produce green bodies for sintering.

The modified air-compatible UHS setup is shown in Fig. 1a and S1.† Two coils made of kanthal (Fe–Cr–Al alloy) are mounted on a fixture composed of two ceramic screws. A pressed green-body pellet was sandwiched between two kanthal coils, and the coils are connected with a B&K Precision 9103 DC power supply to provide intense Joule heating for pellet sintering. In a typical sintering experiment, a 25 V, 12 A DC current was applied to the heating elements (~6 A current passing through each coil), enabling the pellet to be heated up to 1200 °C within 30 seconds. The heater power was turned off after reaching the targeted dwell time, and the pellets were naturally cooled down, which generally took around 1 min to reach room temperature. To realize even faster cooling for the microstructural evolution study, compressed air was blown to the heater fixture once the DC power is turned off, enabling the sample to cool down to room temperature within 10 seconds. The pellets were then polished with SiC grinding papers to remove the top 0.2 mm for XRD measurement, and further polished up to 1200 grit to reach a shiny flat surface. The pellets were subjected to energy dispersive X-ray spectroscopy analysis to confirm no Fe, Cr or Al impurities exist (Table S1†).

Powder XRD measurements were performed with a Bruker D8 X-ray diffractometer, with an increment of 0.05° and a scanning speed of 1 step per second. The Rietveld refinement of XRD data is processed with a Fullprof Software package. The SEM images were obtained with a FEI Quanta 200 FEG Environmental-SEM. The EIS experiments were processed with a BioLogic electrochemical workstation, with both sides of the pellets coated with silver paste and heated at 100 °C for 30 min for ion-blocking cell fabrication, and the data were fitted with RelaxIS impedance analysis software. The Li|LZP|Li cells were assembled by attaching two pieces of Li metal foil on both sides of the polished LZP pellets in an Ar-filled glove box, and a piece of Cu foil was attached on each side of the pellet to serve as the current collector. The cell was then placed in a home-made pressure cell set, and 5 MPa pressure was applied with a zig with screws and springs. The pressurized cells are finally placed in an air-tight secondary chamber, and placed in a thermal chamber operating at 50 °C to process symmetric cell cycling at 0.05 mA cm^{-2} and an areal capacity of 0.05 mA h cm^{-2} with a Landt battery cycler.

Data availability

The data supporting this article have been included as part of the ESI.† Data include all temperature dependent impedance spectroscopy data and experimental details are included for synthesis and experimental apparatus design.

Conflicts of interest

There are no conflicts to declare.

Acknowledgements

The authors thank the support from the Office of Naval Research Young Investigator Program through grant number N00014-23-1-2047. The authors acknowledge the use of Princeton's Imaging and Analysis Center (IAC), which is partially supported by the Princeton Center for Complex Materials (PCCM), a National Science Foundation (NSF) Materials Research Science and Engineering Center (MRSEC; DMR-2011750).

References

1 T. Krauskopf, F. H. Richter, W. G. Zeier and J. Janek, Physicochemical concepts of the lithium metal anode in solid-state batteries, *Chem. Rev.*, 2020, **120**, 7745–7794.
2 S. Randau, D. A. Weber, O. Kötz, R. Koerver, P. Braun, A. Weber, E. Ivers-Tiffée, T. Adermann, J. Kulisch, W. G. Zeier, *et al.*, Benchmarking the performance of all-solid-state lithium batteries, *Nat. Energy*, 2020, **5**, 259–270.
3 F. Zheng, M. Kotobuki, S. Song, M. O. Lai and L. Lu, Review on solid electrolytes for all-solid-state lithium-ion batteries, *J. Power Sources*, 2018, **389**, 198–213.
4 K. B. Hatzell, X. C. Chen, C. L. Cobb, N. P. Dasgupta, M. B. Dixit, L. E. Marbella, M. T. McDowell, P. P. Mukherjee, A. Verma, V. Viswanathan, *et al.*, Challenges in lithium metal anodes for solid-state batteries, *ACS Energy Lett.*, 2020, **5**, 922–934.
5 L. Lin, A. Ayyaswamy, Y. Zheng, A. Fan, B. S. Vishnugopi, P. P. Mukherjee and K. B. Hatzell, Nonintuitive Role of Solid Electrolyte Porosity on Failure, *ACS Energy Lett.*, 2024, **9**, 2387–2393.
6 M.-G. Jeong, K. B. Hatzell, S. Banerjee, B. S. Vishnugopi and P. P. Mukherjee, Temperature Impact on Lithium Metal Morphology in Lithium Reservoir-Free Solid-State Batteries, *PRX Energy*, 2024, **3**, 023003.
7 J. Janek and W. G. Zeier, Challenges in speeding up solid-state battery development, *Nat. Energy*, 2023, **8**, 230–240.
8 K. B. Hatzell and Y. Zheng, Prospects on large-scale manufacturing of solid state batteries, *MRS Energy Sustainability*, 2021, **8**, 33–39.
9 M. B. Dixit, W. Zaman, Y. Bootwala, Y. Zheng, M. C. Hatzell and K. B. Hatzell, Scalable manufacturing of hybrid solid electrolytes with interface control, *ACS Appl. Mater. Interfaces*, 2019, **11**, 45087–45097.
10 M. B. Dixit, B. S. Vishugopi, W. Zaman, P. Kenesei, J.-S. Park, J. Almer, P. P. Mukherjee and K. B. Hatzell, Polymorphism of garnet solid electrolytes and its implications for grain-level chemo-mechanics, *Nat. Mater.*, 2022, **21**, 1298–1305.
11 M. B. Dixit, M. Regala, F. Shen, X. Xiao and K. B. Hatzell, Tortuosity effects in garnet-type Li7La3Zr2O12 solid electrolytes, *ACS Appl. Mater. Interfaces*, 2018, **11**, 2022–2030.
12 C. Wang, W. Ping, Q. Bai, H. Cui, R. Hensleigh, R. Wang, A. H. Brozena, Z. Xu, J. Dai, Y. Pei, *et al.*, A general method to synthesize and sinter bulk ceramics in seconds, *Science*, 2020, **368**, 521–526.
13 K. Liu, J.-T. Ma and C.-A. Wang, Excess lithium salt functions more than compensating for lithium loss when synthesizing Li6. 5La3Ta0. 5Zr1. 5O12 in alumina crucible, *J. Power Sources*, 2014, **260**, 109–114.
14 T. Clemenceau, N. Andriamady, P. K. MK, A. Badran, V. Avila, K. Dahl, M. Hopkins, X. Vendrell, D. Marshall and R. Raj, Flash sintering of Li-ion conducting ceramic in a few seconds at 850 °C, *Scr. Mater.*, 2019, **172**, 1–5.
15 C.-M. Chang, Y. I. Lee, S.-H. Hong and H.-M. Park, Spark plasma sintering of LiTi2 (PO4) 3-based solid electrolytes, *J. Am. Ceram. Soc.*, 2005, **88**, 1803–1807.
16 K. Suzuki, K. Noi, A. Hayashi and M. Tatsumisago, Low temperature sintering of Na1+ xZr2SixP3- xO12 by the addition of Na3BO3, *Scr. Mater.*, 2018, **145**, 67–70.
17 Y. Lai, Z. Sun, L. Jiang, X. Hao, M. Jia, L. Wang and F. Liu, Rapid sintering of ceramic solid electrolytes LiZr2 (PO4) 3 and Li1. 2Ca0. 1Zr1. 9 (PO4) 3 using a microwave sintering process at low temperatures, *Ceram. Int.*, 2019, **45**, 11068–11072.
18 J. E. Iglesias and C. Pecharromán, Room temperature triclinic modification of NASICON-type LiZr2 (PO4) 3, *Solid State Ionics*, 1998, **112**, 309–318.
19 M. Catti, S. Stramare and R. Ibberson, Lithium location in NASICON-type Li+ conductors by neutron diffraction. I. Triclinic α-LiZr2 (PO4) 3, *Solid State Ionics*, 1999, **123**, 173–180.
20 S. Hasegawa, N. Imanishi, T. Zhang, J. Xie, A. Hirano, Y. Takeda and O. Yamamoto, Study on lithium/air secondary batteries—Stability of NASICON-type lithium ion conducting glass–ceramics with water, *J. Power Sources*, 2009, **189**, 371–377.
21 W. Zaman, L. Zhao, T. Martin, X. Zhang, Z. Wang, Q. J. Wang, S. Harris and K. B. Hatzell, Temperature and pressure effects on unrecoverable voids in Li metal solid-state batteries, *ACS Appl. Mater. Interfaces*, 2023, **15**, 37401–37409.
22 H. El-Shinawi, A. Regoutz, D. J. Payne, E. J. Cussen and S. A. Corr, NASICON LiM 2 (PO 4) 3 electrolyte (M= Zr) and electrode (M= Ti) materials for all solid-state Li-ion batteries with high total conductivity and low interfacial resistance, *J. Mater. Chem. A*, 2018, **6**, 5296–5303.
23 M. Catti, N. Morgante and R. Ibberson, Order–disorder and mobility of Li+ in the β-and β-LiZr2 (PO4) 3 ionic conductors: A neutron diffraction study, *J. Solid State Chem.*, 2000, **152**, 340–347.
24 M. Catti, A. Comotti and S. Di Blas, High-temperature lithium mobility in α-LiZr2 (PO4) 3 NASICON by neutron diffraction, *Chem. Mater.*, 2003, **15**, 1628–1632.
25 H. Fukuda, S. Kusakawa, K. Nakano, N. Tanibata, H. Takeda, M. Nakayama, M. Karasuyama, I. Takeuchi, T. Natori and Y. Ono, Bayesian optimisation with transfer learning for NASICON-type solid electrolytes for all-solid-state Li-metal batteries, *RSC Adv.*, 2022, **12**, 30696–30703.
26 Y. Li, W. Zhou, X. Chen, X. Lü, Z. Cui, S. Xin, L. Xue, Q. Jia and J. B. Goodenough, Mastering the interface for advanced all-solid-state lithium rechargeable batteries, *Proc. Natl. Acad. Sci. U. S. A.*, 2016, **113**, 13313–13317.
27 H. El-Shinawi, C. Greaves and J. Janek, Sol–gel synthesis and room-temperature properties of α-LiZr 2 (PO 4) 3, *RSC Adv.*, 2015, **5**, 17054–17059.
28 H. Xu, S. Wang, H. Wilson, F. Zhao and A. Manthiram, Y-doped NASICON-type LiZr2 (PO4) 3 solid electrolytes for lithium-metal batteries, *Chem. Mater.*, 2017, **29**, 7206–7212.
29 A. Loutati, P. Odenwald, B. Aktekin, J. Sann, O. Guillon, F. Tietz and D. Fattakhova-Rohlfing, Survey of Zirconium-Containing NaSICON-type Solid-State Li+ Ion Conductors with the Aim of Increasing Reduction Stability by Partial

Cation Substitution, *Batteries Supercaps*, 2022, **5**, e202200327.

30 L. Jiang, Y. Liao, Q. Wan and W. Li, Effects of sintering temperature and particle size on the translucency of zirconium dioxide dental ceramic, *J. Mater. Sci.: Mater. Med.*, 2011, **22**, 2429–2435.

31 A. Wonisch, T. Kraft, M. Moseler and H. Riedel, Effect of different particle size distributions on solid-state sintering: a microscopic simulation approach, *J. Am. Ceram. Soc.*, 2009, **92**, 1428–1434.

32 R. Marder, R. Chaim, G. Chevallier and C. Estournès, Densification and polymorphic transition of multiphase Y2O3 nanoparticles during spark plasma sintering, *Mater. Sci. Eng., A*, 2011, **528**, 7200–7206.

33 S.-J. L. Kang, *Sintering: Densification, Grain Growth and Microstructure*, Elsevier, 2004.

34 P. Badkar and J. Bailey, The mechanism of simultaneous sintering and phase transformation in alumina, *J. Mater. Sci.*, 1976, **11**, 1794–1806.

35 S. J. Wu, L. C. De Jonghe and M. N. Rahaman, Sintering of nanophase γ-Al2O3 powder, *J. Am. Ceram. Soc.*, 1996, **79**, 2207–2211.

36 M. Nakayama, K. Nakano, M. Harada, N. Tanibata, H. Takeda, Y. Noda, R. Kobayashi, M. Karasuyama, I. Takeuchi and M. Kotobuki, Na superionic conductor-type LiZr 2 (PO 4) 3 as a promising solid electrolyte for use in all-solid-state Li metal batteries, *Chem. Commun.*, 2022, **58**, 9328–9340.